Pergamon
www.elsevier.com/locate/asr
PII: S0273-1177(01)00110-7
Adv. Space Res. Vol. 27, No. 4, pp. 687–692, 2001

Printed in Great Britain
0273-1177/01 $20.00 + 0.00

ORIGIN OF COSMIC RAY ELECTRONS

S.A. Stephens[1]

[1]*Department of Physics, University of Tokyo, 7-3-1 Hongo, Bunkyo-ku, Tokyo 113-0033, Japan,*

ABSTRACT

Positrons (e^+) in cosmic radiation are believed to be produced by the interactions of cosmic ray nuclei with interstellar space. e^+ production spectrum had been calculated using a new set of invariant cross sections for the production of pions and kaons. In the case of e^-, a primary component had been added to the secondary e^- produced along with e^+ in the galaxy. The equilibrium spectra of both e^+ and e^- were obtained and compared with the observations. An empirical relation is given for the energy loss rate due to inverse-Compton scattering, which connects smoothly the Thompson and Klein-Nishina regimes. It is found that a simple power law injection spectrum for e^- can not explain the observed $[e^+/(e^+ + e^-)]$ ratio, and one requires a spectral flattening below about 8 GeV. Flat e^- spectrum similar to that in Crab supernova with a spectral break by one power around 5 GeV could explain both the observed spectrum and the $[e^+/(e^+ + e^-)]$, suggesting that the sources of cosmic ray e^- are supernovae energized by pulsars.

INTRODUCTION

Though electron component constitutes only about one percent of the total cosmic radiation, it provides a valuable tool to understand the propagation of cosmic rays and the physical state of the space where cosmic rays spent most of their time. This stems from the fact that electrons being light leptons, suffer severe energy loss, by which their energy spectrum is considerably modified during propagation in the Galaxy. The major energy loss processes they undergo are different from those of the nucleonic components. Below 1 GeV, Bremsstrahlung process is important and the radiation arising from this process contributes to a large fraction of the non-thermal background radiation in the γ-ray regime. At higher energies, the dominant energy loss mechanisms are the synchrotron radiation and inverse-Compton scattering, while traversing ambient magnetic and radiation fields respectively. While the energy loss due to these processes is proportional to the square of the electron energy, the former one leads to the emission of non-thermal radio background in the Galaxy over a broad band of frequencies and the latter one elevates the energy of ambient photons to X and γ-ray energies. Thus, the knowledge of the electron component plays an important role in the understanding of the origin and propagation of cosmic rays, as well as on the origin of non-thermal radiation and the physical state of the region where this radiation comes from.

The electron component consists of both positive and negative particles. They are the end products of the decay of unstable particles, like pions and kaons, which are produced by the interaction of cosmic ray nucleons with the interstellar gas. If this process is the major source of e^+ and e^-, it is expected that the abundance of e^+ and e^- should be nearly equal, with a small positive excess. However, the observations clearly show a large excess of e^-, suggesting that most of the observed e^- are of primary origin. Estimates of the production spectrum of e^+ in the Galaxy were carried out in the past (eg: Daniel & Stephens, 1975; Protheroe, 1982; Moskalenko & Strong, 1998). The production spectrum was re-examined in this investigation, by parameterizing the invariant cross-sections for the production of pions and kaons in proton-proton collisions. Knowing the e^+ production spectrum, one could determine the equilibrium spectrum using propagation models and applying all energy loss mechanisms accurately. In this context, an attempt was made to connect the energy loss rate through inverse-Compton scattering between the two regimes, namely, the Thompson limit and the extreme Klein-Nishina limit. A comparison of the calculated equilibrium spectrum was then made with the observations after applying solar modulation. At high energies, where

solar modulation does not modify the spectrum, it provides information on the propagation including physical state of the propagating region. At low energies where modulation is important, this compo gives the absolute magnitude of the modulation. These aspects are described in this paper.

The observed spectrum of e^- is steeper than that of the nucleonic component and it is essential to the type of production spectrum of e^- and the sources which produce them. Therefore, different of input production spectrum for e^- had been used in this investigation and the equilibrium spectra determined using the propagation and modulation parameters, obtained from the e^+ investigation. calculated spectra were then compared with the observation to draw important conclusions relating origin of electrons in cosmic rays. These deductions were cross-checked using the $[e^+/(e^+ + e^-)]$ as a func of energy.

PRODUCTION OF SECONDARY ELECTRONS

Major part of the electrons produced by the collisions of cosmic-ray nuclei with the interstellar ma (ISM) comes from the decay of pions. In order to calculate the spectra of pions and kaons resulting from cosmic-ray interactions, it is essential to determine the equilibrium spectra of cosmic- ray nucleon compo This was obtained in the frame work of leaky-box model as described by Stephens and Streitmatter (19 In this investigation, I made use of the latest cross-sections given by Webber (private communication employed time as the variable, rather than the matter traversal. Calculations were carried out for H, D, ^{4}He, C and O nuclei by incorporating all other heavy nuclei as equivalent to C and O. It was assumed the injection spectral shape of primary nuclei is a power law in rigidity with a spectral index of -2.32. resultant spectra of p, He, C and O were subjected to solar modulation and compared with the obse data. This was needed to make sure that there was no error due to normalization.

The cosmic-ray nucleons in the ISM were considered to be bare nucleons and were grouped under prot and neutrons, by using the calculated spectra and the charge to mass ratio of all nuclei (Stephens Streitmatter, 2000). The production spectra of pions and kaons were then determined by making use the inclusive invariant cross-section for producing them ($Ed^3\sigma/dp^3$). The parameterization of $Ed^3\sigma/dp^3$ the production of pions in p-p collisions has the following form, which provides a good fit to the data projectile momentum above 6.6 GeV/c.

$$\frac{Ed^3\sigma}{dp^3} = Aw(s)(1 - X_R)^{z(p_t)} exp[-Bw'(s)p_t]$$

where X_R is the ratio of total energy of the particle to the available energy in the center of mass sys s is the square of the total 4-momenta of the projectile and the target, s_{th} the threshold value of s, and the transverse momentum. The functions w(s), w'(s) and z(p_t) are defined below.

$$w(s) = A_1(1 - s_{th}/s)^{-A_2} \quad for \quad s_{th}/s \geq C_1$$
$$= 1.0 \quad for \quad s_{th}/s < C_1 \qquad (1a)$$
$$w'(s) = B_1(s/4m_p^2)^{B_2} \quad for \quad s \leq C_2$$
$$= 1.0 \quad for \quad s > C_2 \qquad (1b)$$
$$z = D_1 - D_2 p_t + w(p_t) \qquad (1c)$$
$$w(p_t) = D_3[p_t^2 - 0.81] \quad for \quad p_t > 0.9\,GeV/c$$
$$= 0.0 \quad for \quad p_t \leq 0.9\,GeV/c \qquad (1d)$$

In the case of kaons, the parameterization obtained by Badhwar and Stephens (1977) was used. The consta required for the above equation are given in Table 1. The procedure used to carry out the calculations the above parameterization are given below. It was assumed that $(Ed^3\sigma/dp^3)_{\pi^+}$ in p-p collision is the sa as for $(Ed^3\sigma/dp^3)_{\pi^-}$ in n-p collisions. This assumption was extended to kaons. The error resulting neglecting associate production of K^+ near threshold energies is negligible, as the contribution from k at these energies is very small. Though the ISM contains only 10% helium by number, the effect of momentum of target nucleons is important and it had been incorporated (Stephens, 1997). Muon spe from the decay of pions and kaons were obtained using two body decay kinematics. In the case of k

Table 1. Constants

	A	A_1
π^+	99.0	0.35
π^-	72.5	0.72
π^0	93.0	0.57

only the channel from muon decay The calculated are shown in Figu helium abundance e^- is about 5. Thi energies. The asy needs to examine of electrons by kn

PROPAGATIO

Leaky-box mod ing the propagati

$$\frac{\partial N(E,t)}{\partial t} =$$

The first term on t scattering. The in case of ionization ionized hydrogen a of the continuous e to the different co escape time T^{es} h as determined fro (Stephens and Str

In the case of i Klein-Nishina limi

$$\frac{dE}{dt} = 1.0184$$
$$= 3.605$$

Here, $< \epsilon >$ and ρ One can notice fro well below 14.6/ < with star light pho these two regions i

$$\frac{dE}{dt} = 6.313$$

This expression pr change-over energi The steady stat $\partial N(E)/\partial t \rightarrow 0$. I

Table 1. Constants in the set of equations (1)

	A	A_1	A_2	B	B_1	B_2	C_1	C_2	D_1	D_2	D_3
e^+	99.0	0.35	2.65	4.60	0.3	0.6	0.35	26	4.0	1.45	1.2
e^-	72.5	0.72	0.90	4.10	0.0	0.0	0.31	-	5.0	0.9	0.27
e^0	93.0	0.57	1.82	4.35	0.0	0.0	0.27	-	4.5	1.2	0.75

ly the channel $K \longrightarrow \mu + \nu$ was considered with proper branching ratio. Finally, the electron spectrum om muon decay was evaluated and results for energies > 10 MeV are given.

The calculated production spectra of e^+ and e^- resulting from the collisions of cosmic-ray nuclei with ISM e shown in Figure 1. They are given per unit hydrogen density in the ISM, which takes into account the lium abundance also, as described earlier. These spectra peak at about 30 MeV, where the ratio of e^+ to $^-$ is about 5. This ratio decreases on either side of the peak, reaching an asymptotic value of 1.4 at large ergies. The asymptotic spectral slope is approximately the same as that of the cosmic ray nucleons. One eeds to examine at low energies, the role of delta production, the target nucleus effect and the production f electrons by knock-on process.

PROPAGATION OF ELECTRONS

Leaky-box model had been used for the propagation of the electron component, and the equation describ- ng the propagation can be written as (Stephens, 1990)

$$\frac{\partial N(E,t)}{\partial t} = \frac{\partial}{\partial E}\left\{N(E,t)\frac{dE}{dt}\right\} - \int_0^1 \left[N(E) - N(\frac{E}{1-v},t)\right]\psi_{rad}(v)dv - \frac{N(E,t)}{T^{es}(E)} + Q(E,t) \qquad (2)$$

The first term on the RHS is the energy loss term, consisting of ionization, synchrotron and inverse-Compton scattering. The integral term is for the Bremsstrahlung loss, which is not a continuous energy loss. In the case of ionization and Bremsstrahlung, the composition of ISM, consisting of 80% neutral hydrogen, 10% ionized hydrogen and 10% helium nuclei, had been taken into account. Further, proper derivatives in energy of the continuous energy loss term had been carefully incorporated for the different expressions corresponding to the different composition. The next term is due to particle escape from the confinement region and the escape time T^{es} has a constant value of $T_0^{es} = 30$ Myr below 2.7 GV and is $T_0^{es}(2.7/E)^{0.5}$ above 2.7 GV, as determined from the abundance of radio clock nuclei (Streitmatter and Stephens, 2000) and B/C ratio (Stephens and Streitmatter, 2000).

In the case of inverse-Compton scattering, the energy loss in the two regions, Thompson limit and the Klein-Nishina limit, are given here (Blumental and Gould, 1970).

$$\frac{dE}{dt} = 1.0184 \times 10^{-16} E^2 \rho[1.0 - 0.03425E < \epsilon >]GeV/s \qquad for \quad E \leq 14.599/ < \epsilon > \qquad (3)$$

$$= 3.605 \times 10^{-12} \frac{\rho}{< \epsilon >^2}[ln(E < \epsilon >) - 7.1525]GeV/s \qquad for \quad E \geq 3193.3/ < \epsilon > \qquad (4)$$

Here, $< \epsilon >$ and ρ are the mean energy and the energy density of the photons in eV and eV/cc respectively. One can notice from the above equations, that in the Thompson limit, the energy loss is proportional to E^2 and below $14.6/ < \epsilon >$ GeV and there is a large gap between these two regions. In the case of scattering with star light photons, the E^2 dependence is valid only below about a GeV. The empirical fit that connects these two regions is,

$$\frac{dE}{dt} = 6.313 \times 10^{-16} \frac{\rho}{< \epsilon >^2}[E < \epsilon >]^{1.061} GeV/s \qquad for \quad 14.599/ < \epsilon > \leq E \leq 3193.3/ < \epsilon > \qquad (5)$$

This expression provides the missing link between these two extreme regions, and the derivatives at the change-over energies show good continuity.

The steady state solution to the Eq.(2) was obtained by the method of Runge- Kutta technique until $\partial N(E)/\partial t \rightarrow 0$. In this equation, the production term Q(E) is described in the previous section. For this

calculation, the interstellar density of hydrogen was taken to be 0.2 atom/cc corresponding to Two Myr (Streitmatter and Stephens, 2000), as obtained from the study of radio-clock isotopes. The value the effective perpendicular component of the interstellar magnetic field was taken to be 3 μ G. This includes the variation over the regions in the halo, where cosmic rays are confined. Similarly, the star density was taken to be 0.3 eV/cc. I have also considered a case, in which the mean magnetic field and photon density were assumed to be 5 μ G and 0.5 eV/cc respectively, representing the values in the Disk large energies, where lifetime due to energy loss is small, one needs to consider the effect of nearby sources This can not be examined by using the leaky-box model and requires the solution of diffusion equation in space and time.

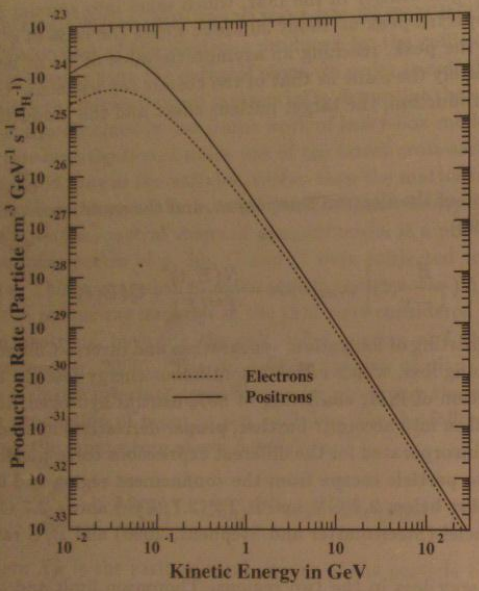

Fig. 1. The calculated production spectra of electrons and positrons in the ISM from the interaction of cosmic ray nuclei are shown per unit n_H.

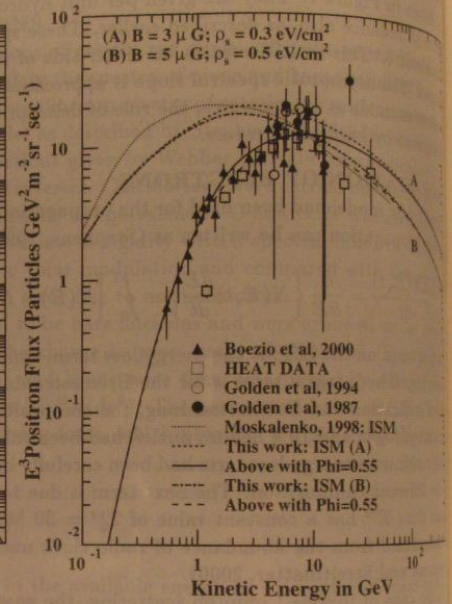

Fig. 2. The calculated positron spectra are compared with the observation. The flux values are multiplied by E^3. The upper curves are for the interstellar spectra while the lower ones are at the Earth.

RESULTS

Positron spectrum

The observed positron spectrum measured during the last two decades is shown in Figure 2. The values in this figure are multiplied by E^3. Only CAPRICE results (Boezio et al, 2000) are available below a few GeV and one can notice considerable spread in the data above about 4 GeV. In this figure and the two figures the combined HEAT data (Barwick et al, 1998) are plotted as reported by Muller(2000). The short-dashed curve marked as A and the dash-dotted curve marked as B in this figure are the interstellar spectra obtained from this calculation for the two sets of energy loss parameters describing the extent of confinement, which includes a part of the Halo (Curve A), and the Disk (Curve B) . They differ at low energies due to the change in the physical state of the region, relating to magnetic field and star light photon density. These spectra also differ from that of Moskalenko and Strong (1998) at low energies, due to the difference in the estimated production spectra, and at high energies due to the propagation effects.

ulated spectra are shown by the solid and long-dashed Curves A and B. Spherically symmetric model was for the solar modulation and the curves in the figure correspond to an equivalent modulation parameter 500 MV. It can be seen that both the modulated Curves A and B agree with the observation within the certainties of the measurements. It is clear from this figure that one needs to measure the e^+ spectrum curately at high energies in order to distinguish between different models, whether the observed positrons ve their time mostly inside the disk (Curve B) or they stay mostly in the extended halo region (Curve A). the following investigation, the physical parameters relevant to the extended confinement region, which respond to Curves marked as A in Figure 1, are only used.

ctron spectrum

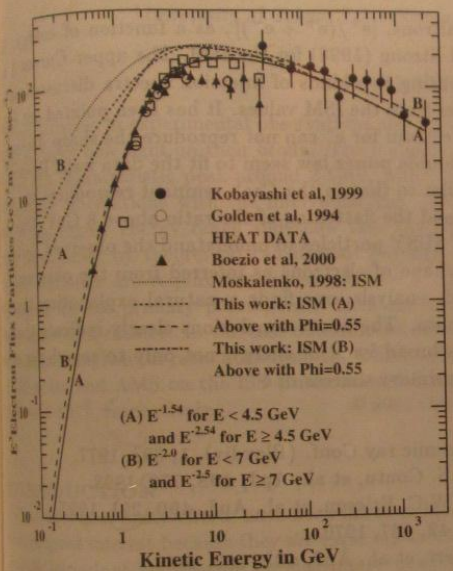

Fig. 3. The calculated electron spectra are compared with the observation. The flux values are multiplied by E^3. The upper curves are spectra in the ISM and the lower ones are spectra near the Earth.

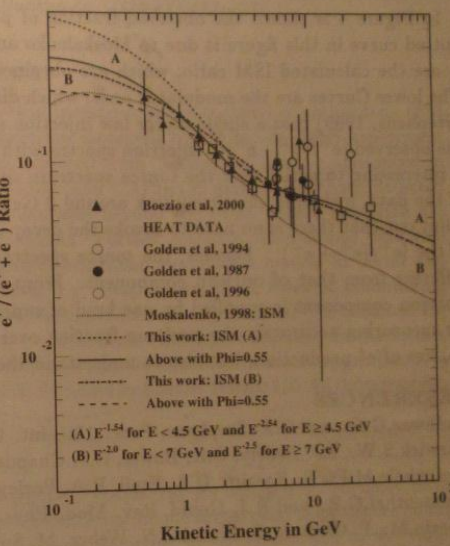

Fig. 4. The calculated $[e^+/(e^+ + e^-)]$ by various models are compared with the observation.

The electron spectrum measured during the last two decades is plotted in Figure 3. As in the case of , the flux values are multiplied by E^3. There is large scatter of data above 7 GeV. It has been shown ier that one could fit the observed e^- spectrum using a simple power law injection spectrum with a slope of -2.4 (Stephens, 1999). However, this required a larger modulation parameter than for the e^+. The served non-thermal radio spectrum in the Galaxy indicates that the electron spectrum in the ISM should become much flatter below about a few GeV (eg: Daniel and Stephens, 1975; Rockstroh and Webber, 1978). Therefore, injection spectra which flatten below a few GeV had been examined. In the first case, a spectrum of the type, $80E^{-2.0}$ electrons / (m^2.sr.s.GeV), which is the production spectrum multiplied by T_0^{ea}, 4π and was used for $E \leq 7$ GeV. This spectrum was assumed to steepen to a slope of -2.5 above 7 GeV. The resulting equilibrium spectrum is shown by Curves B in Figure 3, along with the modulated spectrum, using the same absolute modulation as in the case of e^+. One can notice that the spectrum fits the data well. However, it is hard to explain a spectral break of $\Delta\beta = 0.5$ from a source. Therefore, an alternate source spectrum was also considered in this investigation.

In the case of pulsar driven supernova remnants, like the Crab nebula, the electron spectrum in the ... is very flat. The relationship between the radio spectral index, α, and the electron spectral index, ... $\beta = 1 + \alpha$. Since the radio spectral index of Crab nebula is -0.27 (Bietenholz et al., 1997), an equiv... source spectrum of the type, $50E^{-1.54}$ electrons / (m^2.sr.s.GeV) for $E \leq 4.5$ GeV was considered, wh... steepen by one power above this energy due to energy loss at the source. The resultant equilibrium spectr... is shown by dash-dotted Curve A in Figure 3 and the modulated spectrum is shown by solid Curve A, wh... fit the data well. For a comparison, the estimated e^- spectrum in the ISM by Moskalenko and Strong (19... is also shown. This appears to be steeper at lower energies than both types of spectra considered in ... investigation. As in the case of e^+, one needs to improve the quality of e^- observation beyond about 7 G... to remove possible systematic uncertainty and to draw very meaningful deductions.

Positron fraction

In Figure 4 is shown the observed fraction of positrons, $[e^+/(e^+ + e^-)]$, as a function of energy. T... dotted curve in this figure is due to Moskalenko and Strong (1998) for the ISM. The upper Curves A a... B are the calculated ISM ratio, which are obtained using two kinds of injection spectra discussed earl... The lower Curves are the modulated ones, which differ from the ISM values. It has been pointed out earl... (Stephens, 1999) that a single power law injection spectrum for e^- can not reproduce the sharp decrease... the observed $[e^+/(e^+ + e^-)]$. Injection spectra with double power law seem to fit the data well. However, ... is interesting to notice that the source spectrum similar to that in the Crab remnant reproduces the tre... of the data, including the sharp kink around 3 GeV and the flattening of the ratio above 8 GeV. One m... point out that there is no need to invoke the decay of SUSY particles to understand the observed flatteni... of the $[e^+/(e^+ + e^-)]$. Further, the source spectral shape of electrons as inferred from the observation... different from that of nucleon component. From this analysis, one finds a natural explanation that t... electron component is supplied by one kind of supernova. The above conclusions clearly indicate the pr... for measuring accurately the positron fraction over a broad band of energy, not only to search for exo... sources of e^+ production, but also to understand the primary sources of e^-.

REFERENCES

Badhwar,G.D., and S.A. Stephens, Proc. 15th Int. Cosmic ray Conf. (Plovdiv), **1**, 398, 1977.

Barwick,S.W., J.J. Beatty, C.R. Bower, C.J. Chaput, S. Coutu, et al., ApJ, **498**, 779, 1998.

Bietenholz,M.F., N. Kassim, D.A. Frail, R.A. Parley, W.C. Ericson, et al., ApJ, **490**, 291, 1997.

Blumenthal,G.R., and R.J. Gould, Rev. Mod. Phys., **42**, 237, 1970.

Boezio,M., P. Carlson, T. Francke, N. Weber, M. Suffert, et al., ApJ, **532**, 653, 2000.

Daniel,R.R., and S.A. Stephens, Sp. Sci. Rev., **17**, 45, 1975.

Golden,R.L., B.G. Mauger, G.D. Badhwar, R.R. Daniel, J.L. Lacy, S.A. Stephens, et al., ApJ, **287**, ... 1984.

Golden,R.L., S.A. Stephens, B.G. Mauger, G.D. Badhwar, R.R. Daniel, et al., A&A, **188**, 145, 1987.

Golden,R.L., C. Grimani, B.L. Kimbell, S.A. Stephens, S.J. Stochaj, et al., ApJ, **436**, 769, 1994.

Golden,R.L., S.J. Stochaj, S.A. Stephens, F. Aversa, G. Barbiellini, et al., ApJ, **457**, L103, 1996.

Kobayashi, T., J. Nishimura, Y. Komori, T. Shirai, N. Tateyama, et al., Proc. 26th Int. Cosmic ray Co... (Salt Lake City), **3**, 61, 1999.

Moskalenko,I.V, and A.W. Strong, ApJ, **493**, 694, 1998.

Muller,D., in this issue, 2000.

Rockstroh,J.M., and W.R. Webber, ApJ, **224**, 677, 1978.

Stephens,S.A., Proc. 21st Int. Cosmic Ray Conf. (Adelaide), **11**, 99, 1990.

Stephens,S.A., Astropart. Phys., **6**, 229, 1997.

Stephens,S.A., Proc. 26th Int. Cosmic Ray Conf. (Salt Lake City), **4**, 241, 1999.

Stephens,S.A., and R.E. Streitmatter, ApJ, **505**, 266, 1998.

Stephens,S.A., and R.E. Streitmatter, in this issue, 2000.

Streitmatter,R.E., and S.A. Stephens, Proc. 26th Int. Cosmic Ray Conf. (Salt Lake City), **4**, 199, 19...

Streitmatter,R.E., and S.A. Stephens, in this issue, 2000.